Application of Autoregressive Spectral Analysis to Cepstral Estimation of Mean Scatterer Spacing

Keith A. Wear, Robert F. Wagner, *Fellow, IEEE*, Michael F. Insana, *Member, IEEE*, and Timothy J. Hall, *Member, IEEE*

Abstract—**The problem of estimation of mean scatterer spacing in an object containing regularly spaced structures is addressed. An autoregressive (AR) spectral estimation method (based on Burg's algorithm) is compared with a conventional fast Fourier transform (FFT) based approach for this task. Regularly spaced structures produce a periodicity in the power spectrum of ultrasonic backscatter. This periodicity is manifested as a peak in the cepstrum. A phantom was constructed for comparison of the two methods. This phantom contained regularly spaced nylon filaments. In addition, it contained randomly positioned glass spheres that produced incoherent backscatter. In an experiment in which this target was interrogated using broadband ultrasound, the AR spectral estimate offered considerable improvement over the FFT when the analysis gate length was on the order of the structural dimension. Advantages included improved resolution, reduction in bias and variance of scatterer spacing estimates, and greater resistance to ringing artifacts. Data was also acquired from human liver *in vivo*. AR spectral estimates on human data exhibited a decreased dependence on gate length. These results offer promise for enhanced spatial resolution and accuracy in ultrasonic tissue characterization and nondestructive evaluation of materials.**

I. Introduction

ULTRASONIC SCATTERING from the human liver has two principal components. One component, which is highly coherent, is due to scatterers (probably lobules or portal triads) that are spaced at relatively regular intervals. The other component, which is highly incoherent, is due to more randomly situated scatterers (possibly individual cells) [1]–[7].

One feature that has been successfully utilized in the characterization of diffuse liver disease is the average spacing between scatterers associated with the coherent component of the backscattered signal. This parameter may be derived from spectra of broadband radio frequency (RF) signals corresponding to backscattered ultrasound. Reflections from neighboring scatterers interfere constructively at certain frequencies (for which the intervening distance is equal to an integer number of half wavelengths), in a manner similar to Bragg scattering. This effect is manifested as a set of peaks in the power spectrum. The interscatterer spacing may be computed from the location of the fundamental peak or from the spacing of adjacent harmonics.

Manuscript received December 16, 1991; revised April 10, 1992, and September 3, 1992; accepted September 3, 1992.

K. A. Wear and R. F. Wagner are with the Food and Drug Administration, Center for Devices and Radiological Health, HFZ-142, 1270 Twinbrook Parkway, Rockville, MD 22852.

M. Insana and T. Hall are with the University of Kansas Medical Center, 39th and Rainbow Boulevard, Kansas City, KS 66103.

IEEE Log Number 9204722.

Fellingham and Sommer [4] successfully used mean scatterer spacing to differentiate normal (mean=1.07 mm, standard deviation=0.16 mm, fourteen subjects) from cirrhotic (mean=1.48 mm, standard deviation=0.24 mm, 15 patients) liver. They also had success in the spleen, differentiating normal subjects from those with lymphoma. Their algorithm was based on detection of peaks in the autocorrelation of the power spectral densities of RF signals. Garra and coworkers [1] used mean scatterer spacing in their multifeature classification of diffuse liver disease.

Spectral estimates in the examples given previously were based on fast Fourier transforms (FFT's) of digitized RF signals. (The squared modulus of the FFT is often referred to as the *periodogram*). However, the FFT has severe limitations in some cases. In particular, if small gate lengths are used, the FFT exhibits a considerable compromise in resolution in the frequency domain. The FFT may be expressed as the convolution of the true Fourier transform of the signal with the Fourier transform of the time gate function. Smaller gates result in greater distortion of spectral estimates. This effect was negligible for the gate lengths used by Fellingham and Sommer [4] (1 cm) and Garra *et al.* [1] (3 cm). If better resolution than 1 cm is desired, however, the FFT may be inadequate.

Autoregressive-moving average (ARMA) techniques for spectral estimation offer an alternative to the periodogram [8]. Compared with classical techniques, these methods can provide superior spectral resolution. They have been applied in many fields, including radar, seismology, oil exploration, speech processing, Doppler ultrasound, radiography, magnetic resonance spectroscopy, and stock market forecasting [8]–[15]. Their relative advantage over the FFT increases with decreasing gate length.

Some elementary definitions regarding ARMA models and scatterer spacing estimation is presented in Section II. In addition, the technique of estimating scatterer spacing from the cepstrum is discussed. In Section III, data acquisition and analysis methods and results are described for a phantom experiment and for a human experiment. Applications of these results in ultrasonic tissue characterization are discussed in the final section.

II. Theory

A. The ARMA Model

An autoregressive-moving average (ARMA) model for a sampled signal $x[n]$ is given by [8] where the first sum

corresponds to the autoregressive (AR) portion

$$x[n] = -\sum_{k=1}^{p} a[k]x[n-k] + \sum_{k=0}^{q} b[k]u[n-k] \qquad (1)$$

and the second corresponds to the moving average (MA) portion. The term *autoregressive* refers to a linear sum of previous (regressive) samples of the output process itself (auto). The MA portion is a filtered version of an input sequence, $u[k]$, which is assumed to be a white noise process with mean zero and variance ρ. The AR coefficients are $a[k]$ and the MA coefficients are $b[k]$. By convention, $b[0] = 1$. The integers p and q are referred to as the *orders* of the AR and MA portions respectively. For a pure MA model, $p = 0$. (That is, the first sum in (1) disappears). For a pure AR model, $q = 0$. (Note that for a pure AR model, the $k = 0$ term of the second summation remains).

The power spectral density may be obtained from the squared modulus of the Fourier transform of (1). The power spectral density of the input white noise sequence is $\rho\Delta t$ where ρ is the variance of $u[k]$ and Δt is the sampling interval.

$$P_{\mathrm{ARMA}}(f) = \rho\Delta t|B(f)/A(f)|^2 \qquad (2)$$

where

$$A(f) = 1 + \sum_{k=1}^{p} a[k]e^{-j2\pi fk\Delta t} \qquad (3)$$

and

$$B(f) = 1 + \sum_{k=1}^{q} b[k]e^{-j2\pi fk\Delta t}. \qquad (4)$$

The exponentials arise from applying the Fourier shift theorem to the delayed samples of $x[n]$ and $u[n]$ in (1). For a pure AR model, $B(f) = 1$.

The zeros of $A(z)$ (where $z = e^{-j2\pi f\Delta t}$) produce poles in the complex z plane and therefore peaks in the power spectrum. Sharp peaks in a spectrum corresponding to resonances from regularly spaced scatterers may be attributed to poles in an AR model. For spectra containing deep nulls, but no sharp peaks, Marple recommends using a pure moving average model [8, ch. 6].

B. Determination of Autoregressive Coefficients

The AR coefficients, $a[k]$, and the white noise variance, ρ, may be obtained from the autocorrelation sequence, $r[m]$, of the process $x[n]$ [8]. A set of linear equations that relate $a[k]$, ρ, and $r[m]$ may be obtained by multiplying (1) by its complex conjugate and then taking the ensemble average. These equations are referred to as the AR Yule–Walker normal equations. Solution of this set of equations is expedited by application of a recursive method known as Levinson's algorithm [8]. If $x[n]$ is a Gaussian process and $r[m]$ is known exactly, then the power spectrum obtained in this way is equivalent to the *maximum entropy* spectral estimate provided that the Shannon–Burg measure of entropy is used rather than the Gibbs–Jaynes measure [16]. This is the spectrum that is associated with the most unpredictable time series consistent with the known values of the autocorrelation function. In practice, $r[m]$ is not known exactly but is estimated from measurements. Solution of the Yule–Walker equations using an estimate for $r[m]$ obtained from data provides a method for obtaining approximate values for the AR coefficients, and therefore an approximate power spectral density. Another method for estimating the AR coefficients, known as Burg's algorithm, involves calculating $a[k]$ directly from measurements of $x[n]$ (without estimation of the autocorrelation sequence $r[m]$). This method is described in great detail elsewhere [8], [9].

C. Estimation of Scatterer Spacing Using the Cepstrum

Regularly spaced structures produce peaks in the power spectrum of ultrasonic backscatter. Reflections from neighboring scatterers interfere constructively at certain frequencies (for which the spacing is equal to an integer number of half wavelengths). The peaks occur at frequencies given by $f = nc/2d$ where f denotes frequency, n is an integer, d is the scatterer spacing, and c is the speed of sound. The factor of 2 results from reflection imaging geometry.

The quality of scatterer spacing estimates is directly related to spectral peak detectability. Other characteristics of the spectrum, such as center frequency, or full width half maximum, etc. are relatively unimportant for this task. As discussed in Section II-A, sharp peaks in the power spectrum (poles in the complex z plane) may be associated with the autoregressive portion of the model (see (1)–(4). Hence, in this study, a pure AR model was used for spectral estimation.

A robust method for determining interscatterer spacing is by identification of the location of the peak in the cepstrum. The cepstrum is defined as the Fourier transform of the logarithm of the power spectral density [17]–[19]. A periodicity in the spectrum (that is, a set of equally spaced sharp resonances or a set of equally spaced nulls) will produce a peak in the cepstrum. The use of the cepstrum for the estimation of scatterer spacing in medical ultrasonic applications was introduced by Lizzi, Fellepa, and co-workers at the Riverside Research Institute [19]. They used the cepstrum to measure hepatic vessel wall thickness.

The utility of the cepstrum may be illustrated by the following simple example that is based on the discussion by Oppenheim and Schafer [17, ch. 10]. Consider a process, $x(t)$, which may be represented as the convolution of an impulse response, $p(t)$ (which here incorporates the electromechanical characteristics of the transducer, diffraction, and attenuation), and a function that describes tissue scattering, $r(t)$:

$$x(t) = p(t) * r(t). \qquad (5)$$

Consider two identical scatterers separated by a distance d:

$$r(t) = s(t + t_0) + s(t + t_0 + 2d/c) \qquad (6)$$

where c is the speed of sound. The power spectrum of the received signal is then

$$|X(f)|^2 = |P(f)|^2|S(f)|^2|1 + e^{-j2\pi f(2d/c)}|^2. \qquad (7)$$

Taking the logarithm (the next step toward computing the cepstrum):

$$\log|X(f)|^2 = \log|P(f)|^2 + \log|S(f)|^2 + 2\log|1 + e^{-j2\pi f(2d/c)}|. \qquad (8)$$

The last term is periodic with period equal to $c/2d$. Upon Fourier transformation (the final step toward computing the cepstrum) this periodicity will manifest itself as a peak at $t = 2d/c$. Assuming that the transfer function, $P(f)$, and the frequency dependent backscatter, $S(f)$, do not vary dramatically over changes of frequency on the order of $c/2d$, their contributions to the cepstrum will be confined to times much smaller than $2d/c$.

III. Experiment

A. Data Acquisition

In order to test the algorithm, a custom phantom was constructed. The phantom consisted of glass spheres (mean diameter = 75μm) embedded in agar. The number density of the spheres was 3 per mm^3. The speed of sound in the phantom was measured to be 1540 m/s. Also present in the phantom was a grid of parallel nylon lines. The grid spacing was 2.54 mm. Thus, the nylon lines provided coherent backscatter from regularly spaced reflectors while the glass spheres provided incoherent backscatter.

The phantom was interrogated with an unfocused, circular (0.5-in diameter) Panametrics A3029 transducer. The center frequency was 2.25 MHz. The -20-dB bandwidth was 1.5 MHz. A Panametrics 5052UA pulser receiver was used. Received signals were digitized at 25 Msamples/s using a LeCroy TR8828C transient recorder. The transducer was oriented perpendicular to the nylon wires. Forty $A-$lines were acquired from different locations in the phantom.

The spacing interval of 2.54 mm for the nylon lines produced a resonance at 0.3 MHz and harmonics at integer multiples of 0.3 MHz. Since our system transfer function did not vary substantially over changes of frequency on the order of 0.3 MHz, no system response correction was needed for our data.

Human data was acquired using a clinical Diasonics DS-20 mechanical sector scanner. A 3.5-MHz transducer with a 19 mm diameter aperture and full width half maximum (FWHM) bandwidth of approximately 1.0 MHz was used. Data was digitized at 22.1 MHz. A region of interest corresponding to 14 contiguous sector lines, each approximately 3 cm in length was acquired from the human subject.

B. Data Analysis

Spectral estimates as functions of gate length were obtained as follows. Each of the 40 lines of RF (1024 points or 41 μs @ 25 Msamples/s, or 32 mm for $c = 1540$ m/s) was partitioned along its length into n equal segments, 32/n mm long, for $n = 1, 2, 4$, and 8. A spectral estimate (periodogram or AR) was computed for each segment. The cepstrum was then obtained by taking the FFT of the logarithm of the spectral estimate. Scatterer spacing, for each segment, was then estimated from the location of the cepstral peak. When searching for the cepstral peak, the region in which the "ringing peak" (discussed later) was expected was excluded. For each value of $n, 40n$ scatterer spacing estimates were obtained. These values were averaged, in order to estimate the mean and standard deviation of the scatterer spacing estimator.

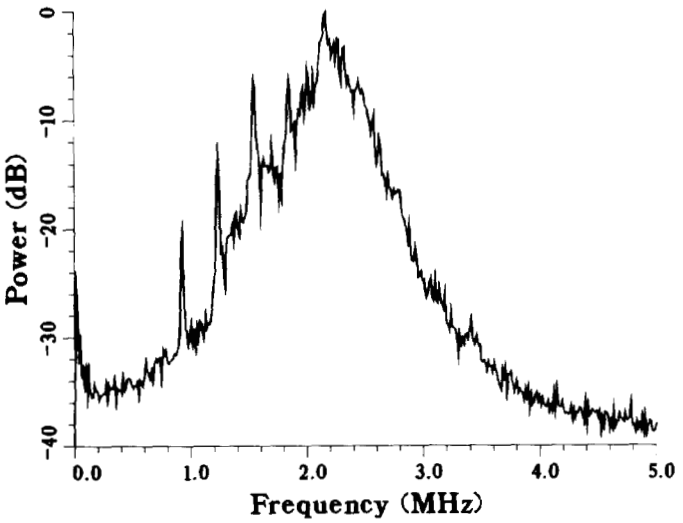

Fig. 1. The average periodogram obtained from 40 lines of RF from the phantom. The gate length was 32 mm. The resonance peaks at 0.9 MHz, 1.2 MHz, and 1.5 MHz correspond to harmonics of a fundamental resonance at 0.3 MHz. These resonances are due to regularly spaced parallel nylon wires in the phantom. The distance between adjacent wires was 2.54 mm.

Periodograms were computed as the squared modulus of the FFT. A rectangular gating function was used. The analysis described above was also repeated using a Hamming window. While the Hamming window reduced ringing artifacts, it degraded spectral resolution, reduced peak conspicuity, and resulted in inferior scatterer spacing estimates.

AR coefficients were obtained using Burg's algorithm. Software included in [8] was used for the computation. Equations (2) and (3) were then used to obtain power spectral estimates from AR coefficients.

The order was chosen such that the model (1) spanned a time interval that corresponded to a distance that was slightly greater than the true scatterer spacing. In this way, any degree of periodicity in the signal $x[n]$, due to the regularly spaced nylon wires, could be reflected in the coefficients, $a[k]$. Thus, selection of a value for p sets an *upper bound* for the values of scatterer spacing detectable by this method. For phantom data, the order was 85 (2.6 mm). For human data, the order ($p = 72$) was chosen such that spacings up to 2 mm could be detected.

For phantom data, corrections for diffraction and the transducer electromechanical response were not necessary (for the reasons outlined in Section II-C). For human liver data, which exhibited a much smaller signal-to-noise ratio (SNR), spectra were divided by the spectrum acquired from a planar interface. Human cepstra exhibited large values corresponding to small (< 1 mm) spacings. These were due to the relatively slowly varying (in frequency domain) contribution from frequency dependent scattering ($S(f)$ in (8)). In order to enhance the cepstral region of principal diagnostic interest (1–2 mm), human liver spectral estimates were high pass filtered.

C. Results

Fig. 1 shows the average periodogram from 40 lines of RF acquired from the phantom. Here the line length was chosen

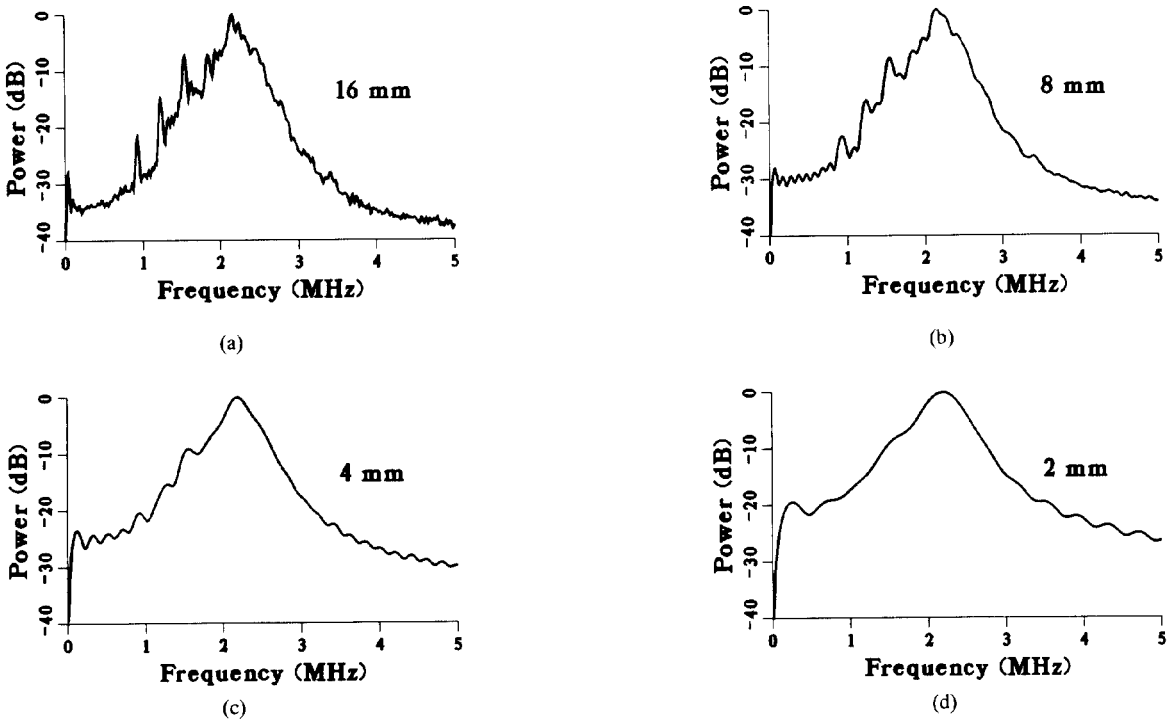

Fig. 2. Average periodograms of RF data obtained from the phantom for four different gate lengths (16 mm, 8 mm, 4 mm, and 2 mm). As the gate length is reduced, three effects are apparent: 1) the peaks become less discernible, 2) estimated noise level increases, and 3) ringing becomes more apparent. (a) 16 mm. (b) 8 mm. (c) 4 mm. (d) 2 mm.

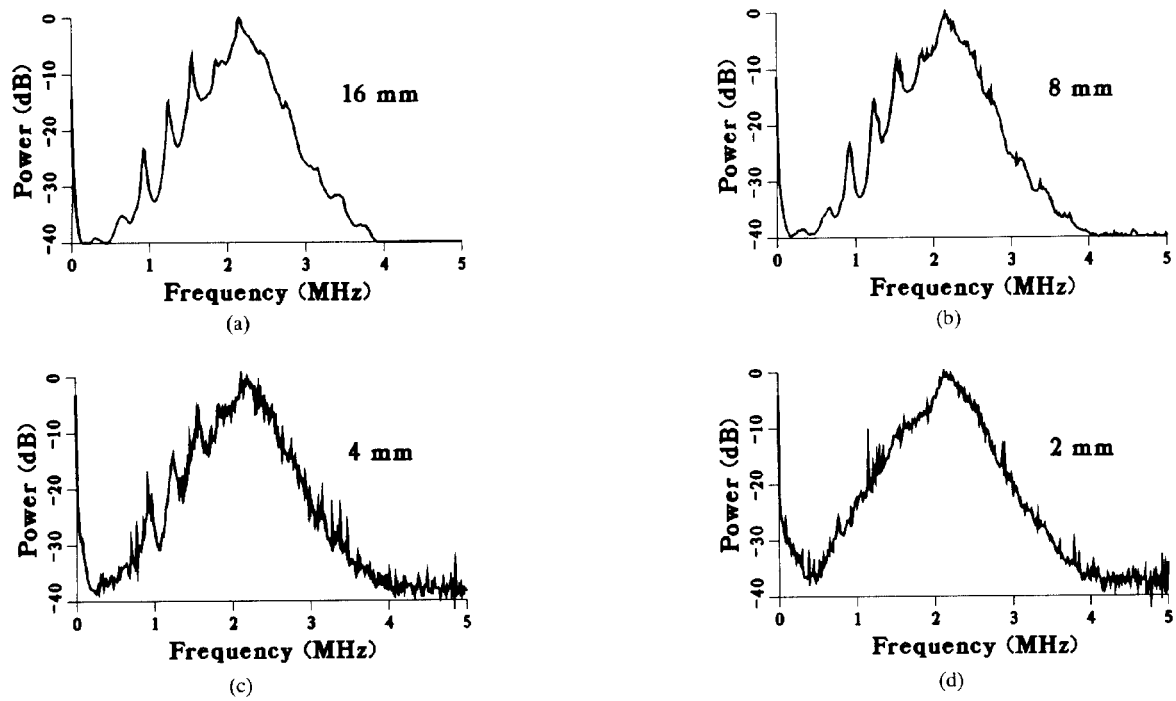

Fig. 3. AR spectral estimates (obtained using Burg's algorithm) of RF data from the phantom for four different gate lengths (16 mm, 8 mm, 4 mm, and 2 mm). For each gate length greater than the actual scatterer spacing (2.54 mm), the resonance peaks are more conspicuous in the AR spectral estimate than in the corresponding periodogram. (a) 16 mm. (b) 8 mm. (c) 4 mm. (d) 2 mm.

to be rather long (1024 points or 41 μs @ 25 Msamples/s, or 32 mm for c = 1540 m/s). This line length would be impractical for imaging applications or for detection of small lesions. However, the corresponding periodogram is relatively free from truncation artifacts and can serve as a standard against which to compare subsequent spectral estimates. This line length resulted in a convolution of the true spectrum with a sinc function with full width half maximum (FWHM) equal to 0.03 MHz, therefore having a small impact on the spectral estimate.

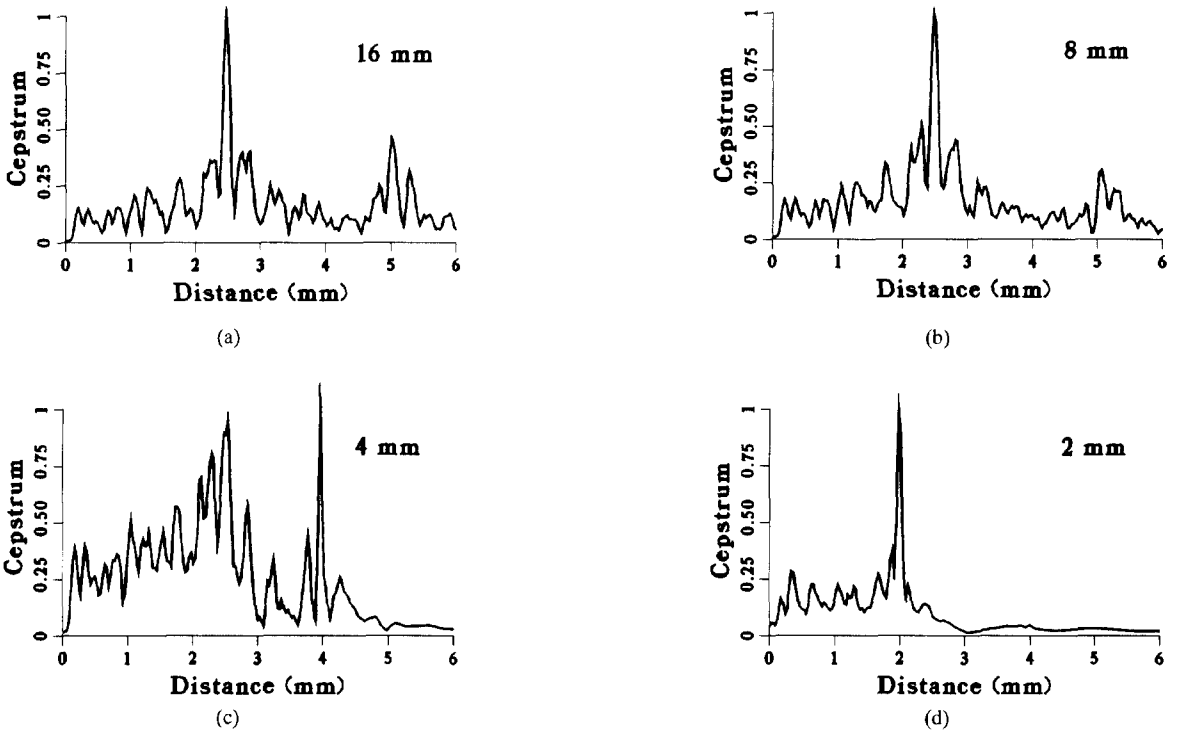

Fig. 4. Average cepstra, based on periodograms, for four different gate lengths (16 mm, 8 mm, 4 mm, and 2 mm). The peak at 2.54 mm is due to the regularly spaced scatterers. The peak at 4 mm for the 4 mm gate and the peak at 2 mm for the 2 mm gate are due to ringing. The peak at 2.54 mm is easily discernible at 16 mm and 8 mm but is much less clear at 4 mm. (a) 16 mm. (b) 8 mm. (c) 4 mm. (d) 2 mm.

Harmonics at 0.9 MHz, 1.2 MHz, 1.5 MHz, 1.8 MHz, and perhaps 2.1 MHz are apparent. The fundamental at 0.3 MHz and the harmonic at 0.6 MHz are lost in the noise. From the spacing between the discernible harmonics, the scatterer spacing may be inferred.

The reduction in peak conspicuity at higher frequencies may be attributed to small variations in the scatterer spacing d. The explanation for this is as follows. Suppose a single irregular pair of scatterers are separated by $d + \Delta d$, rather than the average spacing in the resolution volume, d. For small variations ($\Delta d/d \ll 1$), this irregular pair produces an altered set of resonances that differ from the original set ($f = nc/2d$) by an amount $\Delta f \approx nc\Delta d/2d^2$. As the order (n) increases, the separation (Δf) of the irregular peaks from the main set of peaks *increases* and the degree to which the irregular peaks reinforce the main peaks *decreases*. In this manner, the *rate of decay* of the resonances in the spectrum provides an indication of the *width* of the *distribution* of scatterer spacings in the resolution volume.

In Fig. 2, the effect of decreasing the gate length on the periodogram is shown. The gate lengths of 16, 8, 4 and 2 mm correspond to FWHM of the convolving sinc function of 0.06, 0.12, 0.23, and 0.47 MHz. As the gate length is reduced, the detectability of the peaks decreases. In addition, the estimate of the noise level steadily increases from about -35 dB at 32 mm and 16 mm, to -30 dB at 8 mm, to -25 dB at 4 mm, to -20 dB at 2 mm. At 4 mm, the noise level becomes commensurate with the harmonic at 0.9 MHz. Finally, ringing becomes more apparent as the gate length decreases.

In Fig. 3, AR spectral estimates (based on Burg's algorithm) are shown for the four different gate lengths. At 16 mm, the fundamental at 0.3 MHz is discernible. In addition, harmonics throughout all the usable system bandwidth are apparent. As the gate length is reduced, the spectral estimates become somewhat degraded. However, for each gate length greater than the actual scatterer spacing (2.54 mm), the resonance peaks are more discernible in the AR spectral estimate than in the corresponding periodogram. Moreover, the estimated noise level remains low and does not interfere with the three most prominent peaks at 0.9 MHz, 1.2 MHz, and 1.5 MHz. In addition, ringing is suppressed in the AR estimates.

In Fig. 4, average cepstra, based upon periodogram spectral estimates, for the four different gate lengths are shown. The horizontal axes are calibrated in distance rather than time so that scatterer spacing may be read directly from the graphs. The main peak corresponding to 2.54 mm is clear at 16 mm and 8 mm, somewhat less clear at 4 mm, and, of course, nonexistent at 2 mm. For gate lengths greater than 5 mm (that is, 16 mm and 8 mm) a small peak at 5 mm, due to interference from pairs of wires two intervals apart, is apparent. There are sharp, narrow peaks at 4 mm for the 4 mm gate length and at 2 mm for the 2 mm gate length that are due to ringing.

In Fig. 5, average cepstra, based upon autoregressive spectral estimates, for the four different gate lengths are shown. The peak at 2.54 mm is more discernible, particularly for the 4 mm gate length. Of course, no ringing peaks are evident.

Since scatterer spacing estimation entails *nonlinear* processing of spectra (in particular, peak detection), one cannot

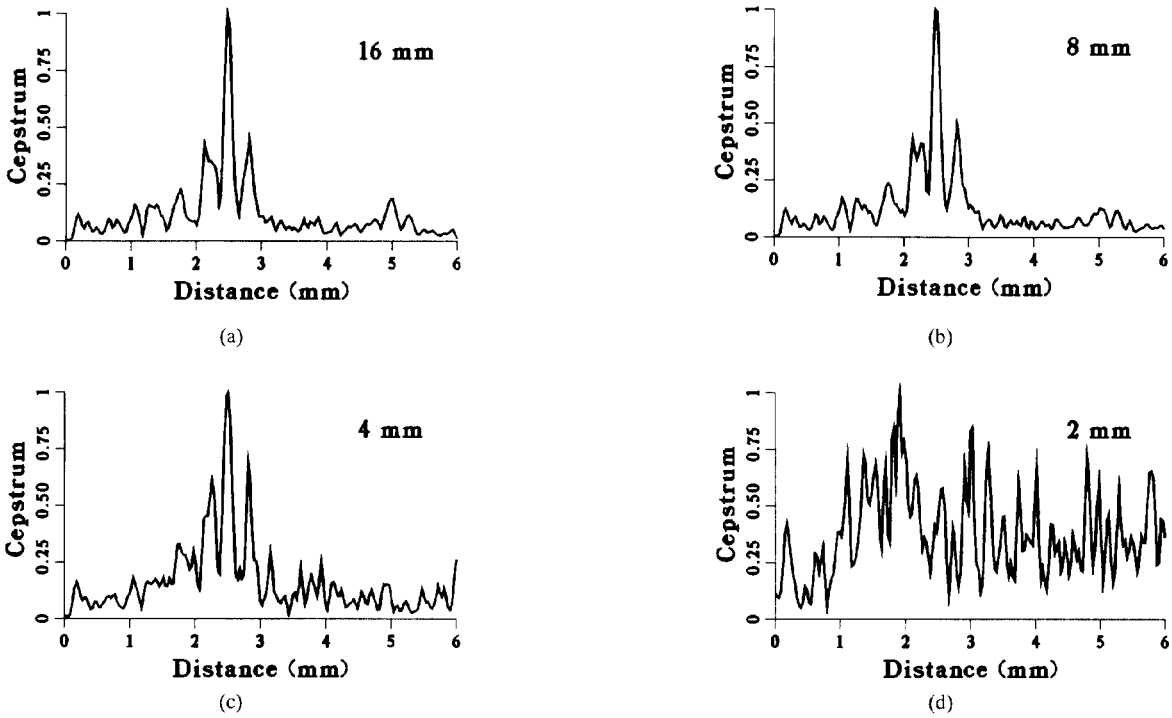

Fig. 5. Average cepstra, based on autoregressive spectral estimates, for four different gate lengths (16 mm, 8 mm, 4 mm, and 2 mm). The peak at 2.54 mm is due to the regularly spaced scatterers. Note that at 4 mm, this peak is much more conspicuous than in the periodogram-based cepstrum (see Fig. 4). (a) 16 mm. (b) 8 mm. (c) 4 mm. (d) 2 mm.

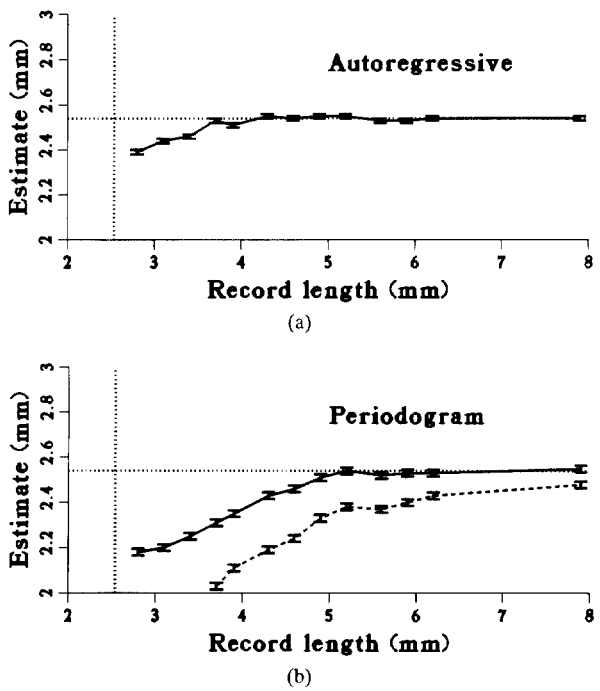

Fig. 6. Scatterer spacing estimates, as functions of gate length, for the two spectral estimation approaches (a) autoregressive and (b) periodogram. The horizontal and vertical dotted lines correspond to the true scatterer spacing (2.54 mm). In (b), the dashed curve corresponds to estimates made using a Hamming window while the solid curve corresponds to estimates made using a rectangular window. The two methods (AR and periodogram with rectangular window) are asymptotically unbiased. However, at small gate lengths, the periodogram based estimate exhibits a larger bias than the AR approach.

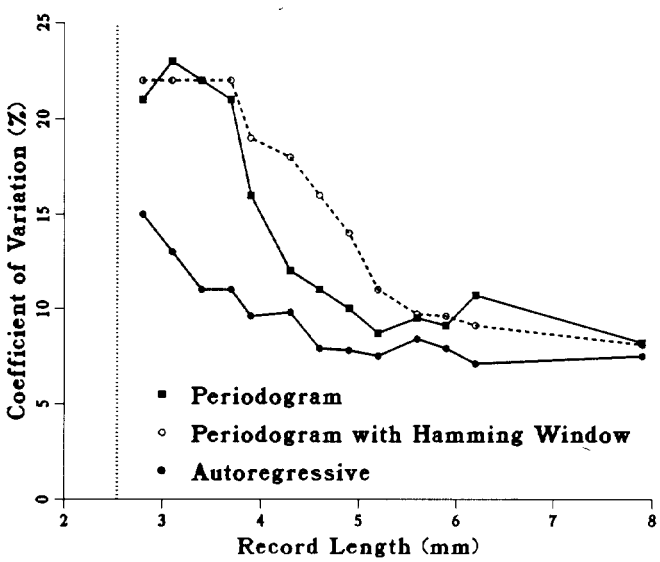

Fig. 7. Coefficients of variation (standard deviation divided by the mean) as functions of gate length.

necessarily expect the average scatterer spacing estimate to correspond to the peak in the average cepstrum. In Fig. 6, estimates of scatterer spacing, as functions of gate length, are shown for both spectral estimation methods. The horizontal and vertical dotted lines correspond to the true scatterer spacing in the phantoms (2.54 mm). (The lower curves illustrate why it is advisable *not* to use the Hamming window). Both methods (autoregressive and periodogram without Hamming window) are asymptotically unbiased. That is, for sufficiently long gate lengths (> two scatterer spacings), the estimates come very close to the true value. However, at small gate lengths (between one and two scatterer spacings), the AR

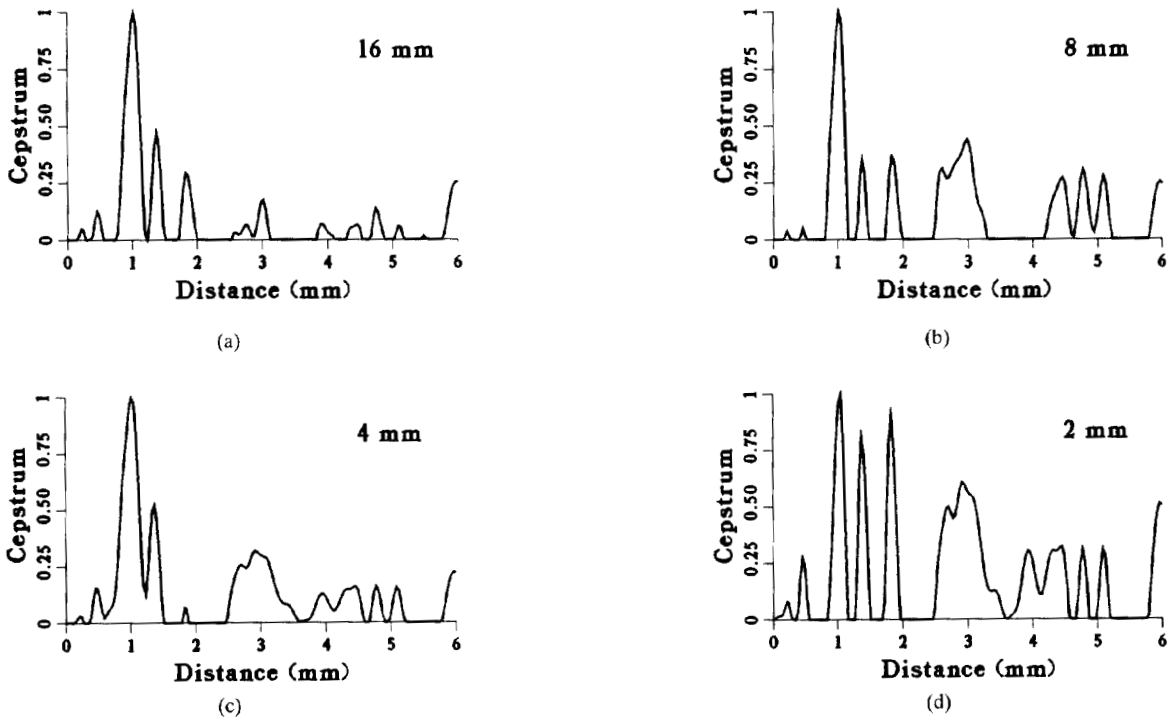

Fig. 8. Ceptra from human *in vivo* liver based on processing with four different gate lengths (32 mm, 16 mm, 8 mm, and 4 mm) using the FFT. The shape of the cepstrum exhibits some dependence on gate length. The main region of diagnostic interest is between 1 and 2 mm. (a) 16 mm. (b) 8 mm. (c) 4 mm. (d) 2 mm.

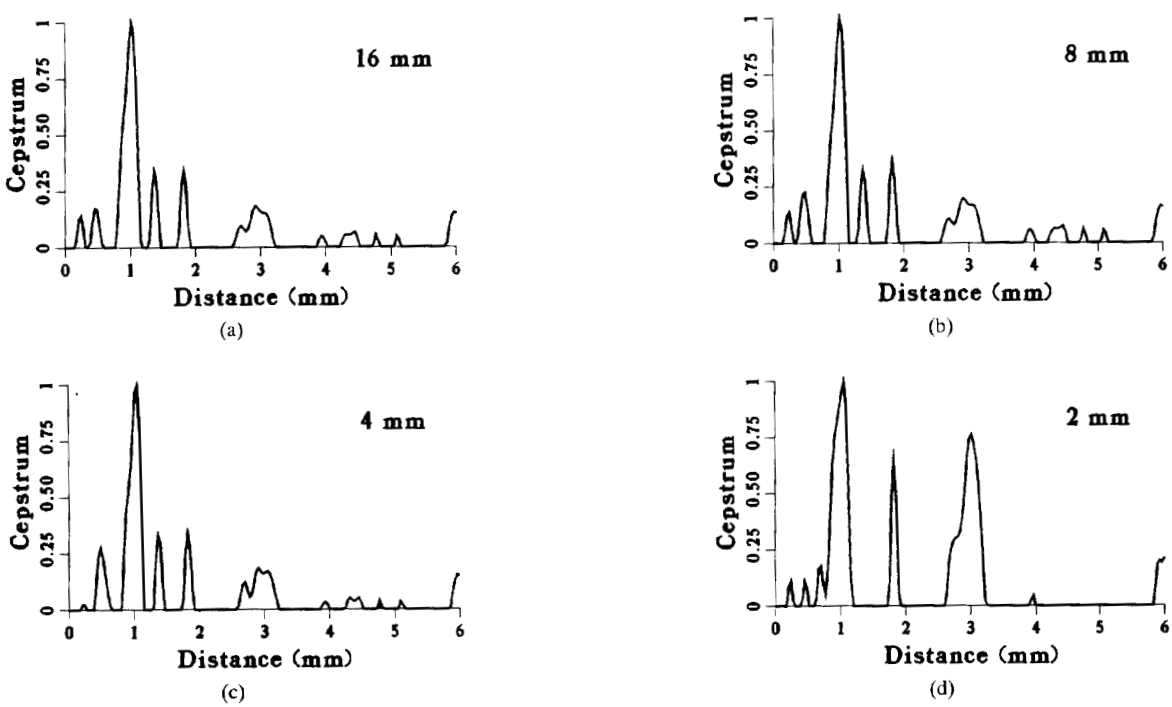

Fig. 9. Cepstra from human *in vivo* liver based on processing with four different gate lengths (32 mm, 16 mm, 8 mm, and 4 mm) using AR spectral estimation. Compared with the FFT-based cepstra, the shape exhibits less dependence on gate length. (a) 16 mm. (b) 8 mm. (c) 4 mm. (d) 2 mm.

approach is much more accurate. Finally, as can be seen in Fig. 7, the AR estimates exhibited a smaller coefficient of variation (standard deviation divided by the mean) than the periodogram-based scatterer spacing estimates.

Cepstra computed from human liver data are shown in Figs. 8 and 9, which are FFT- and AR-based, respectively. The most dominant peak corresponds to a scatterer spacing of approximately 1 mm. At small gate lengths, the FFT-based

cepstra exhibit some variation. At 2-mm gate length, peaks near 1.4 mm and 1.9 mm become competitive with the peak at 1.0 mm, thereby complicating scatterer spacing estimation. The AR-based cepstra are much less sensitive to gate length. From 16 mm down to 4 mm, the AR-based cepstra are virtually unchanged. At 2 mm gate length, some artifacts arise but the peak at 1.0 mm is more discernible than in the FFT-based case.

IV. Conclusion

In addition to randomly positioned scatterers that produce incoherent backscatter, the human liver possesses scatterers that exhibit some degree of regularity and consequently, partially coherent backscatter. Average spacing between these scatterers has been successfully utilized, along with other features, to differentiate normal from diseased liver. Studies reporting this finding have concentrated on characterization of *diffuse* diseases [1], [3], [4]. Measurements have corresponded to average interscatterer spacing over a relatively large volume of tissue. They have been derived from averages of periodograms obtained from RF data with relatively long gate lengths (1–3 cm).

In this paper, an algorithm for improved mean scatterer spacing estimation has been proposed. It was tested on a phantom that contained regularly spaced scatterers with known interscatterer spacing. For this target, the AR spectral estimate (based on Burg's algorithm) offered considerable improvement over the conventional periodogram when the record length was sufficiently small. Advantages included improved resolution, reduction in bias and variance of scatterer spacing estimates, and greater resistance to ringing artifacts. In addition, noise was suppressed.

Often in estimation tasks, it is possible to decrease bias at some cost, usually an increase in variance of estimates. It is important to emphasize that this is not occurring here. With the AR spectral estimation method, a *decrease* in bias of scatterer spacing estimates (Fig. 6) was accompanied by a *decrease* in variance (Fig. 7). The conventional periodogram exhibits a fundamental resolution limit (due to the finite window duration) that leads to the bias in scatterer spacing estimates. The AR spectral estimate does not exhibit this limitation. This property is often referred to as *superresolution* [8].

In the phantom experiment, accurate scatterer spacing estimation was possible even without corrections for electromechanical effects, diffraction, and attenuation. In human tissue, where SNR is smaller, such corrections were found to be necessary.

The level of spatial resolution at which the AR method outperformed the periodogram (< 5 mm) is not essential for detection of diffused diseases. However, it would be essential for detection of a small lesion that is characterized by a difference in mean scatterer spacing relative to the embedding tissue. In addition, creation of images based on spectrally derived features (such as scatterer spacing) may be more feasible with an AR approach.

Acknowledgment

The authors wish to extend thanks to John Burg, Ph.D., for several helpful conversations and to Brian S. Garra, M.D., for assisting in clinical data acquisition.

The mention of commercial products, their sources, or their use in connection with material reported herein is not to be construed as either an actual or implied endorsement of such products by the Food and Drug Administration.

References

[1] B. S. Garra, *et al.*, "Quantitative ultrasonic detection and classification of diffuse liver disease," *Invest. Radiol.*, vol. 24, no. 3, pp. 196–203, Mar. 1989.

[2] R. F. Wagner, M. F. Insana, D. G. Brown, "Statistical properties of radio-frequency and envelope-detected signals with applications to medical ultrasound," *J. Opt. Soc. Amer. A.*, vol. 4, no. 5, pp. 910–922, May 1987.

[3] L. Fellingham-Joynt, "A stochastic approach to ultrasonic tissue characterization," Ph.D. dissertation, Stanford Electron. Lab. SEL 79–023, Tech. Rep. no. g557–4 (Stanford Univ., Stanford, CA, 1979).

[4] L. L. Fellingham and F. G. Sommer, "Ultrasonic characterization of tissue structure in the *in vivo* human liver and spleen," *IEEE Trans. Sonics Ultrason.*, vol. SU-31, pp. 418–428, 1984.

[5] R. F. Wagner, M. F. Insana, and D. G. Brown, "Unified approach to the detection and classification of speckle texture in diagnostic ultrasound," *Opt. Eng.*, vol. 25, pp. 738–742, 1986.

[6] M. F. Insana, R. F. Wagner, B. S. Garra, D. G. Brown, and T. H. Shawker, "Analysis of ultrasound image texture via generalized Rician statistics," *Opt. Eng.*, vol. 25, pp. 743–748, 1986.

[7] M. F. Insana, R. G. Wagner, B. S. Garra, R. Momenan, T. H. Shawker, "Pattern recognition methods for optimizing multivariate tissue signatures in diagnostic ultrasound," *Ultrason. Imag.*, vol. 8, pp. 165–180, 1986.

[8] S. L. Marple. *Digital Spectral Analysis with Applications.* Englewood Cliffs, NJ: Prentice-Hall, 1987.

[9] S. Haykin and S. Kesler, "Prediction-error filtering and maximum-entropy spectral estimation," in *Topics in Applied Physics,* vol. 34, *Nonlinear Methods of Spectral Analysis,* S. Haykin, Ed. Berlin: Springer-Verlag, 1983.

[10] P. J. Vaitkus and R. S. C. Cobbold, "A comparative study and assessment of Doppler ultrasound spectral estimation techniques, Part I: Estimation methods," *Ultrason. Med. Biol.*, vol. 14, no. 8, pp. 661–672, 1988.

[11] P. J. Vaitkus, R. S. C. Cobbold, and K. W. Johnston, "A comparative study and assessment of Doppler ultrasound spectral estimation techniques, part II: methods and results," *Ultrason. Med. Biol.*, vol. 14, no. 8, pp. 673–688, 1988.

[12] F. Forsberg, "On the usefulness of singular value decomposition—ARMA models in Doppler ultrasound," *IEEE Trans. Ultrason. Ferroelec. Freq. Cont.*, vol. 38, pp. 418–428, Sept. 1991.

[13] T. B. Ahn and S. B. Park, "Estimation of mean frequency and variance of ultrasonic Doppler signal by using second-order autoregressive model," *IEEE Trans. Ultrason., Ferroelec., Freq. Cont.*, vol. 38, pp. 172–182, May 1991.

[14] E. A. Trabka and P. C. Bunch, "Application of maximum-entropy spectrum analysis to the measurement of low-frequency radiographic noise spectra," *SPIE*, vol. 454, "Application of optical instrumentation in medicine XII," 1984.

[15] K. A. Wear *et al.*, "Application of parametric spectral estimation to medical ultrasound and magnetic resonance spectroscopy," in *Proc. SPIE Medical Imaging IV Conf.*, vol. 1231, May 1990.

[16] J. Skilling, "Quantified maximum entropy," in *Maximum Entropy and Bayesian Methods,* Paul F. Fougere, Ed. The Netherlands: Kluwer Academic, 1990.

[17] A. V. Oppenheim and R. W. Schafer, *Digital Signal Processing.* Englewood Cliffs, NJ: Prentice-Hall, 1975.

[18] B. P. Bogert, M. J. R. Healy, and J. W. Tukey, "The frequency analysis of time series for echoes: cepstrum, pseudoautocovariance, cross-cepstrum, and saphe cracking," in *Proc. Symp. Time Series Analysis,* M. Rosenblatt, Ed. New York: Wiley, 1963, pp. 209–243.

[19] F. L. Lizzi, E. Feleppa, N. Jaremko, D. King, and P. Wai, "Liver-tissue characterization by digital spectrum and cepstrum analysis," in *Proc. 1981 IEEE Ultrason. Symp.* New York: IEEE, 1981, pp. 575–578.

Keith A. Wear was born in San Diego, CA, in 1957. He received the B.A. degree in applied physics from the University of California at San Diego, in 1980. He received the M.S. and Ph.D. degrees in applied physics from Stanford University, Stanford, CA, in 1982 and 1987.

He was a Research Associate in the Physics Department at Washington University, St. Louis, MO, from 1986 to 1989. Currently, he is a Research Associate at the Food and Drug Administration, Center for Devices and Radiological Health in Rockville, MD. His research interests include ultrasonic tissue characterization and digital signal processing.

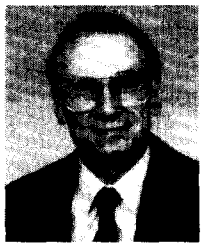

Robert F. Wagner (S'58–M'83–SM'84–F'91) was born in Philadelphia, PA, on January 10, 1939. He received the B.S. degree in electrical engineering in 1959 from Villanova University, Philadelphia, PA, the M.A. degree in 1965 from Augustinian College, Washington, DC, and the M.S. and Ph.D. degrees in nuclear physics in 1965 and 1969, respectively, from Catholic University, Washington, DC.

From 1970 to 1972 he held post-doctoral fellowship at Ohio University, Athens, OH, where he taught modern physics, and did research on photo- and electronuclear interactions. In 1972 he joined the laboratories of the Bureau of Radiological Health (BRH), Rockville, MD, where he has been the Chief of the Diagnostic Imaging Section for the past 15 years. At BRH, which is now the FDA's Center for Devices and Radiological Health, he has worked on problems concerning the ultimate sensitivity of X-ray, CT scanning, and ultrasound systems in medical imaging, vision and image display, and consensus measurement methodology for medical imaging systems. In recent years he has concentrated on machine reading of images, and disease classification using the statistics of image texture. He has published about 10 papers on nuclear physics and about 90 on medical imaging.

Dr. Wagner is a Fellow of the Society for Imaging Science and Technology (formerly SPSE), the SPIE, and the OSA.

Michael F. Insana (M'85), was born in Portsmouth, VA, on December 18, 1954. He received the B.S. degree in physics in 1978 from Oakland University, Rochester, MI, and the M.S. and Ph.D. degrees in medical physics in 1982 and 1983, respectively, from the University of Wisconsin—Madison.

He worked at the Food and Drug Administration, Center for Devices and Radiological Health from 1984 to 1987 as a Research Physicist studying medical techniques. He is currently an Assistant Professor of Radiology at the University of Kansas Medical Center, where he studies signal processing methods in diagnostic ultrasound and conducts signal detection experiments. He is on the editorial board of *Ultrasonic Imaging*.

Dr. Insana is a member of the SPIE, the Acoustical Society of America, the American Institute of Ultrasound in Medicine, the American Association of Physicists in Medicine.

Timothy J. Hall (M'88) received the A.B. degree in physics in 1983 from the University of Michigan—Flint, and the M.S. and Ph.D. degrees in medical physics in 1985 and 1988, respectively, from the University of Wisconsin—Madison.

He joined the Department of Diagnostic Radiology at the University of Kansas Medical Center in 1988, where he is currently an Assistant Professor. His research interests include quantitative ultrasonic imaging, and measures of observer performance and image quality.

Dr. Hall is a member of the Acoustical Society of America and the Society of Photo-Optical Instrumentation Engineers.